

First measurements of remoTES cryogenic calorimeters: easy-to-fabricate particle detectors for a wide choice of target materials

G. Angloher,¹ M.R. Bharadwaj,¹ I. Dafinei,² N. Di Marco,^{3,4} L. Einfalt,^{5,6} F. Ferroni,^{3,2} S. Fichtinger,⁵ A. Filipponi,^{7,4} T. Frank,¹ M. Friedl,⁵ A. Fuss,^{5,6} Z. Ge,⁸ M. Heikinheimo,⁹ K. Huitu,⁹ M. Kellermann,¹ R. Maji,^{5,6} M. Mancuso,¹ L. Pagnanini,^{3,4} F. Petricca,¹ S. Pirro,⁴ F. Pröbst,¹ G. Profeta,^{7,4} A. Puiu,^{3,4} F. Reindl,^{5,6,*} K. Schöffner,^{1,†} J. Schieck,^{5,6} D. Schmiedmayer,^{5,6} C. Schwertner,^{5,6} M. Stahlberg,^{1,‡} A. Stendahl,⁹ F. Wagner,⁵ S. Yue,⁸ V. Zema,^{1,§} and Y. Zhu⁸
(The COSINUS Collaboration)

A. Bento,^{1,10} L. Canonica,¹ and A. Garai¹

¹*Max-Planck-Institut für Physik, 80805 München - Germany*

²*INFN - Sezione di Roma, 00185 Roma - Italy*

³*Gran Sasso Science Institute, 67100 L'Aquila - Italy*

⁴*INFN - Laboratori Nazionali del Gran Sasso, 67010 Assergi - Italy*

⁵*Institut für Hochenergiephysik der Österreichischen Akademie der Wissenschaften, 1050 Wien - Austria*

⁶*Atominstytut, Technische Universität Wien, 1020 Wien - Austria*

⁷*Dipartimento di Scienze Fisiche e Chimiche,*

Università degli Studi dell'Aquila, 67100 L'Aquila - Italy

⁸*SICCAS - Shanghai Institute of Ceramics, Shanghai - P.R.China 200050*

⁹*Helsinki Institute of Physics, Univ. of Helsinki, 00014 Helsinki - Finland*

¹⁰*LIBPhys-UC, Physics Departments, University of Coimbra, 3004-516 Coimbra - Portugal*

(Dated: November 18, 2022)

Low-temperature calorimeters based on a readout via Transition Edge Sensors (TESs) and operated below 100 mK are well suited for rare event searches with outstanding resolution and low thresholds. We present first experimental results from two detector prototypes using a novel design of the thermometer coupling denoted *remoTES*, which further extends the applicability of the TES technology by including a wider class of potential absorber materials. In particular, this design facilitates the use of materials whose physical and chemical properties, as e.g. hygroscopicity, low hardness and low melting point, prevent the direct fabrication of the TES onto their surface. This is especially relevant in the context of the COSINUS experiment (Cryogenic Observatory for SIGNALS seen in Next-Generation Underground Searches), where sodium iodide (NaI) is used as absorber material.

With two remoTES prototype detectors operated in an above-ground R&D facility, we achieve energy resolutions of $\sigma = 87.8$ eV for a 2.33 g silicon absorber and $\sigma = 193.5$ eV for a 2.27 g α -TeO₂ absorber, respectively. RemoTES calorimeters offer – besides the wider choice of absorber materials – a simpler production process combined with a higher reproducibility for large detector arrays and an enhanced radiopurity standard.

I. INTRODUCTION

Low-temperature detectors operated in the temperature region of 10-100 mK make up an important detector class in particle physics. The detection of particles in cryogenic calorimeters is based on the measurement of the tiny temperature increase caused by an energy deposition in an absorber material, by using very sensitive temperature sensors, e.g. Transition Edge Sensors (TESs), Neutron Transmutation Doped-thermistors (NTDs), Kinetic Inductance Detectors (KIDs), or Metallic Magnetic Calorimeters (MMCs).

* Corresponding author, florian.reindl@tuwien.ac.at

† Corresponding author, karoline.schaeffner@mpp.mpg.de

‡ Corresponding author, martin.stahlberg@mpp.mpg.de

§ Corresponding author, vanezema@mpp.mpg.de

A TES consists of a superconductive thin film operated in the state between the normal conducting and the superconducting phase. Due to the strong temperature dependence of the film resistance in the transition, even tiny temperature increases ($\mathcal{O}(\mu\text{K})$) induced by very small energy depositions ($\mathcal{O}(\text{KeV})$) in the absorber, lead to measurable changes in resistance of $\mathcal{O}(10^{-1}\Omega)$. For many decades, TESs have been a main pillar in the scope of cryogenic imaging spectrometers for earth and space applications; their use in the rare event search for direct dark matter detection [1–4] and CE ν NS [5, 6] by using massive absorbers $\mathcal{O}(1\text{-}100\text{ g})$ is a very active field of research at the frontier of knowledge.

TESs based on superconducting tungsten thin-films have been developed within the CRESST dark matter search at the Max-Planck Institute for Physics (MPP) in Munich over the last 30 years. The current stage is CRESST-III, which uses 200 nm-thick tungsten films directly fabricated onto the surface of absorbers made of Al_2O_3 , CaWO_4 , LiAlO_2 and Si. The extraordinary high sensitivity achieved with TESs is one of the cornerstones of CRESST, which is the leading cryogenic experiment for low-mass dark matter search [1, 7].

The deposition of the TES thermometer directly onto the absorber ensures an excellent transmission of the non-thermal phonons to the W-film; it is the preferred solution as long as the absorber material can withstand ¹ the conditions during the involved fabrication steps, i.e. electron-beam evaporation, sputtering, chemical etching and photolithography. However, absorber materials that have a low melting point and/or are hygroscopic cannot undergo these processes. A work-around solution for these delicate materials, such as for the sodium iodide (NaI) crystals used in the COSINUS experiment [4], is the so-called composite design [9]: the TES is fabricated onto a separate substrate named “carrier crystal” which in turn is connected to the absorber via an amorphous interface (glue, oil, or grease). This approach requires the phonons produced by a particle interacting in the absorber to propagate through the interface, the carrier crystal, and finally couple to the TES. A fraction of the signal is lost in this process due to the acoustic mismatch between the different materials of the carrier and the absorber [10]. In COSINUS we used Al_2O_3 , Si, CaWO_4 and CdWO_4 , which all have a high acoustic mismatch to the NaI absorber. Furthermore, in the case of a very good scintillator like NaI, a carrier crystal which is not fully transparent to the scintillation light will reabsorb part of the light, causing an additional power input to the TES. In this case, the resulting pulse shape in the TES will be a superposition of the NaI scintillation signal and the primary thermal signal [11].

In [12], the authors propose a TES-based detector concept, denoted *remoTES* in the following, which does not suffer from these disadvantages, features a simpler production process, and additionally promises a better detector reproducibility. In a *remoTES* detector, the TES is fabricated onto a separate wafer. The absorber crystal is then equipped with a gold pad that transmits the phonon signal created from an interaction in the absorber to the TES via a gold bonding wire. To our knowledge, experimental works using the TES coupling design proposed in [12] are absent to present date. However, the experiment RICOCHET is considering this design to read out superconducting absorbers for precision measurements of coherent elastic neutrino-nucleus scattering (CE ν NS) [13] and the AMORE experiment [14] utilizes thin gold films as phonon absorbers connected to a MMC [15].

Marrying ease of fabrication with a wide choice of absorber materials, the *remoTES* may be a breakthrough for TES-instrumented calorimeters based on delicate absorber materials like NaI. In this article, we present the first experimental implementation and the first results which demonstrate the potential of such detectors.

II. DETECTOR DESIGN

A. Design of the *remoTES*

The design of a *remoTES* detector is schematically depicted in Figure 1. It avoids the carrier crystal by coupling the TES directly to the target crystal via a gold pad connected to a gold bonding wire. A significant advantage of this design is that it eliminates the potential phonon barriers, i.e. the loss of signal due to reflections caused by the acoustic mismatch between absorber crystal, interface and carrier crystal. Even more importantly, phonons directly couple to the electronic system of the gold pad via

¹ Nonetheless the fabrication process might induce stress in the crystal lattice, which is one of the main potential origins of the excess signal at low energies observed in several experiments ([8])

electron-phonon coupling [16]. In the literature, this coupling in gold is found to be comparable to or larger than in tungsten [12, 17–20]. However, the surface and the thickness of the gold pad have to be carefully optimized: a larger surface enhances the phonon collection efficiency and hence the signal amplitude; at the same time a larger volume increases the total heat capacity, reducing the signal amplitude.

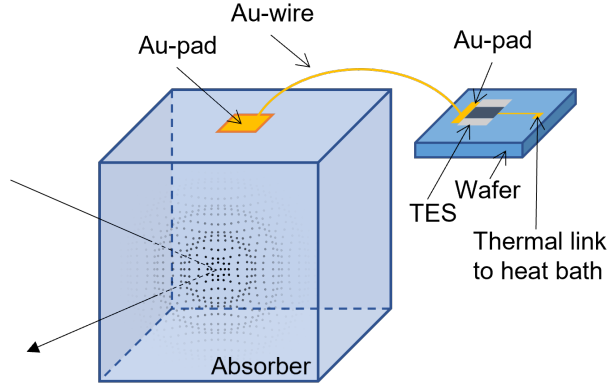


FIG. 1: Schematic view of a *remoTES* detector. The wafer where the TES is fabricated onto (right) is separated from the absorber crystal (left). This crystal is equipped with a gold pad which is linked directly to the TES via a gold bonding wire.

B. Design of two *remoTES*-prototypes

In this manuscript we report the results from two different absorber materials, silicon (Si, 2.33 g) and tellurium dioxide (α -TeO₂, 2.27 g), read out by a *remoTES*. These materials were selected to gain a fundamental understanding of the crucial parameters of this new TES-based readout design. We selected Si as it is a highly-studied standard material for low-temperature application and, thus, useful as a benchmark. We chose TeO₂ as a first step on the way to NaI, mainly for its similar solid-state properties, in particular regarding the heat capacity and the gap between the acoustic and optical phonon modes [21, 22].

Technical details: On the Si absorber ((20x10x5) mm³) a gold film of circular shape (3 mm diameter) of 200 nm thickness was deposited by Magnetron-sputtering. The connection between the Au-pad on the Si absorber and the TES on the wafer was provided via a 17 μ m thick and 2-3 mm long Au-bonding wire. While the Au-wire was wedge-bonded onto the Au-pad of the TES, it was connected to the Au-pad on the Si absorber by using a silver-loaded epoxy (\sim 25 μ g). Avoiding wedge-bonding on the Au-pad of the absorber opens up the possibility to also introduce very soft and fragile absorber crystals to this field of research, which would be damaged by solid phase welding processes (e.g. wedge and ball bonding). Alternatively, the Au-pad on the TeO₂ absorber ((20x10x2) mm³) consists of a 400 nm thick Au-foil glued onto its surface by using a two-component epoxy resin. Using Au-foils which reveal high quality and increased thickness (Residual Resistance Ratio (RRR), listed in Table I), allow to exclude the absorber material from any kind of thin-film deposition processes which require high vacuum conditions. The electrical and thermal contact between Au-pad on the TeO₂ and the TES was realized with a wedge-bond on both sides, respectively. Table I summarizes the condensed information on both prototype detectors.

The TES on the thin Al₂O₃ wafer ((10x10x0.4) mm³) was identical for both measurements. It consists of a 100 nm-thick tungsten film of an area of (220x300) μ m² and two aluminum pads for biasing of the sensor. The area of the W-film not overlapping with the pads is (70x300) μ m². The weak thermal link to the heat bath consists of a 1 mm long Au-stripe (20 μ m in width, 80 nm in thickness).

Absorber material	Si	TeO ₂
Absorber volume (mm ³)	20x10x5	20x10x2
Au-pad properties	200 nm sputtered RRR=3.79	400 nm foil glued RRR=15
Au-wire properties	17 μm glued on pad	17 μm 2 wedge bonds
TES	W-TES on Al ₂ O ₃	W-TES on Al ₂ O ₃
Energy resolution (eV)	87.8 ± 5.6	193.5 ± 3.1

TABLE I: Summary of the two measurements using the *remoTES* design. RRR = Residual Resistance Ratio

III. EXPERIMENTAL RESULTS AND DISCUSSION

The measurements reported here were carried out in a dilution refrigerator of the CRESST group at the Max-Planck Institute for Physics in Munich. This is an above-ground, liquid ⁴He-precooled dilution refrigerator for R&D measurements and TES testing. It is equipped with four SQUID channels (APS company) and a VME-based data acquisition using a hardware-triggered readout. The total exposure was 1.06 g·d for the Si detector and 2.28 g·d for TeO₂. For means of energy calibration both prototype detectors were irradiated by an uncollimated ⁵⁵Fe-source shining onto the bottom side of the absorbers. Furthermore, the TeO₂ detector was equipped with an additional collimated ⁵⁵Fe-source irradiating solely the Au-pad glued onto the absorber.

A. Data analysis

We observe different event classes in both detectors. Standard events (SEVs = averaged pulses scaled to a maximum amplitude of 1 V) for these classes are shown in Figure 2; they were created from a small, selected sample of pulses with the same shape for each class. The most prevalent pulse shape, depicted in green, features a rise time of ~ 1 ms, with a decay time of approximately 44 ms for the Si prototype, and ~ 122 ms for the TeO₂ prototype. The high rate of these events is consistent with hits in the absorber, considering its large mass in comparison with the mass of the wafer carrying the TES. Hits in the latter (orange in Figure 2) occur at a lower rate, and feature much faster signals: the rise times are only 0.16 ms (Si measurement) and 0.07 ms (TeO₂ measurement), while the decay times are ~ 11.2 ms and ~ 1.2 ms, respectively.

The TeO₂ prototype exhibits an additional event class. We identify these comparatively rare events (cf. Table II) as hits from the collimated ⁵⁵Fe-source irradiating the Au-pad on the absorber. The rise time of the pulse is driven by the time needed to transport energy to the TES which depends on the energy carriers. The transport is fast for electrons and non-thermal phonons, which are the dominant energy carriers for the events created by interactions in the Au-pad or the carrier. In the TeO₂ absorber, a larger part of the initial phonon population undergoes thermalization, consequently leading to slower pulses. The Au-pad events are visible in Figure 3a as a cluster of events in the violet box. Their decay time is faster than the one of absorber events, but slower than the one of wafer events. The explanation can be two-fold: firstly, energy deposited in the Au-pad is partially transmitted back and forth to and from the absorber, leading to a larger decay time; secondly, the heat capacity of Au affects the decay time, leading to even slower pulses. As expected, the Au-pad events in Figure 3a are distributed around a larger pulse height (~ 0.07 V) with respect to the pulse height of the ⁵⁵Fe-events in the absorber (~ 0.04 V). A definitive interpretation of the pulse shape requires further studies, which are currently ongoing.

Few basic quality cuts are applied to the complete dataset: events coinciding with a decaying baseline

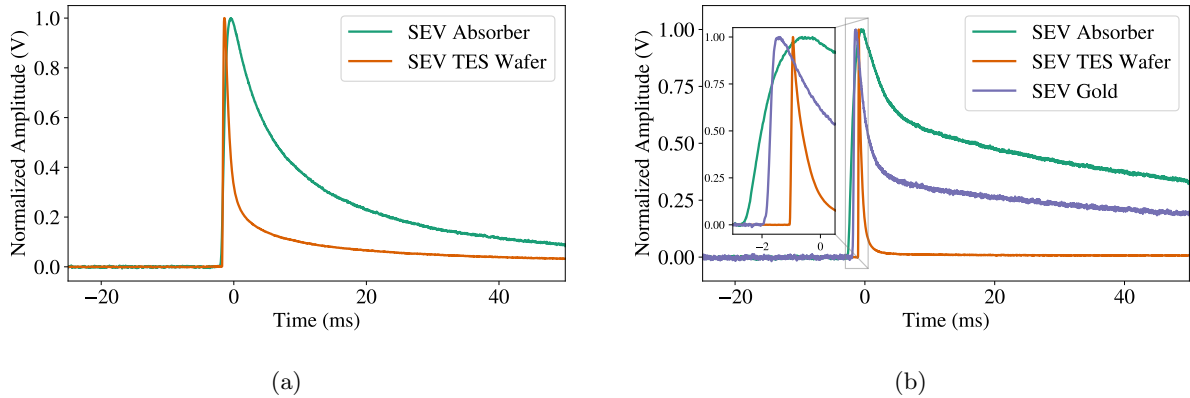


FIG. 2: Standard events (SEVs) for the two prototype detectors. (a) Events in the Si absorber (green) and the TES wafer (orange). (b) Events in the TeO_2 absorber (green), the TES wafer (orange) and the gold pad on the TeO_2 (violet). The pulse onsets for each event class are slightly shifted for visualization purposes.

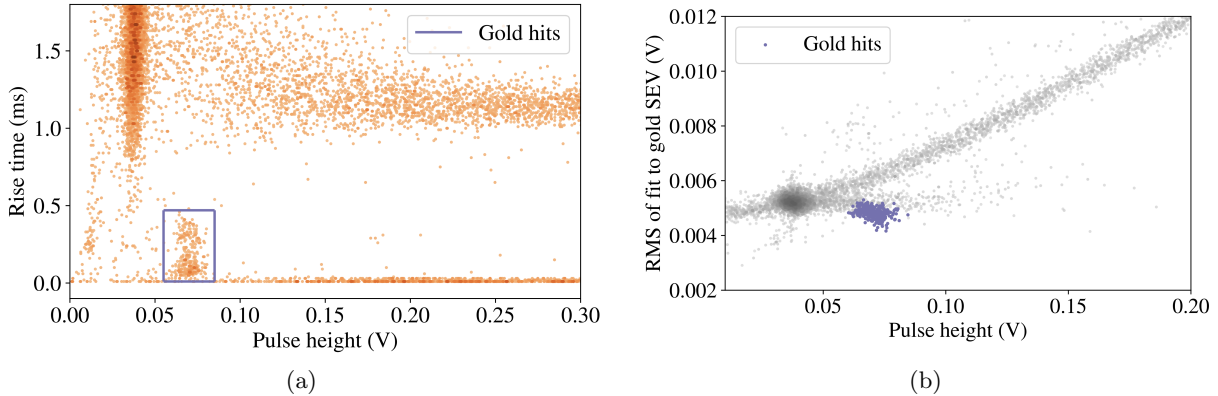


FIG. 3: TeO_2 -*remoTES* data set: (a) Rise time versus moving average pulse height distribution. The violet box encloses the events in the gold foil produced by the collimated ^{55}Fe -source. (b) Fit RMS for the gold SEV as a function of the pulse height distribution. The events from the violet box in panel (a) are tagged and depicted in violet.

from a previous pulse are removed by placing a cut on the pre-trigger baseline slope. Additionally, events with a reconstructed pulse onset more than 1 ms away from the trigger position are discarded. To separate different event classes reliably, the root mean square (RMS) from a truncated standard event fit (see e.g. [7]) is used. We fit each pulse with all three SEVs, and the dataset for each event class contains only those events where the respective fit yields the lowest RMS. As an example, the discrimination between absorber and wafer events is shown in Figure 4. Figure 3 illustrates the discrimination between absorber events and Au-pad events, where the latter are taken from Figure 3a and marked in purple. Table II shows the number of surviving events for each prototype and event class; as stated before, absorber events are the dominant event class in both measurements, and Au-hits are less frequent than wafer hits for the TeO_2 detector.

In addition to the events produced by particles interacting in the active detector parts, we periodically inject electrical pulses with known amplitudes into the heater of each detector. These heater pulses allow monitoring the detector response over time, and accounting for the effect of saturation in the TES, which influences the pulse shape at high energies (see e.g. [7]). A truncated fit with a dedicated heater SEV is performed for all heater pulses, and the resulting amplitude is used in combination with the input pulser setting to compensate non-linearities and time-variations of the reconstructed (fitted) amplitude for particle-induced events [23].

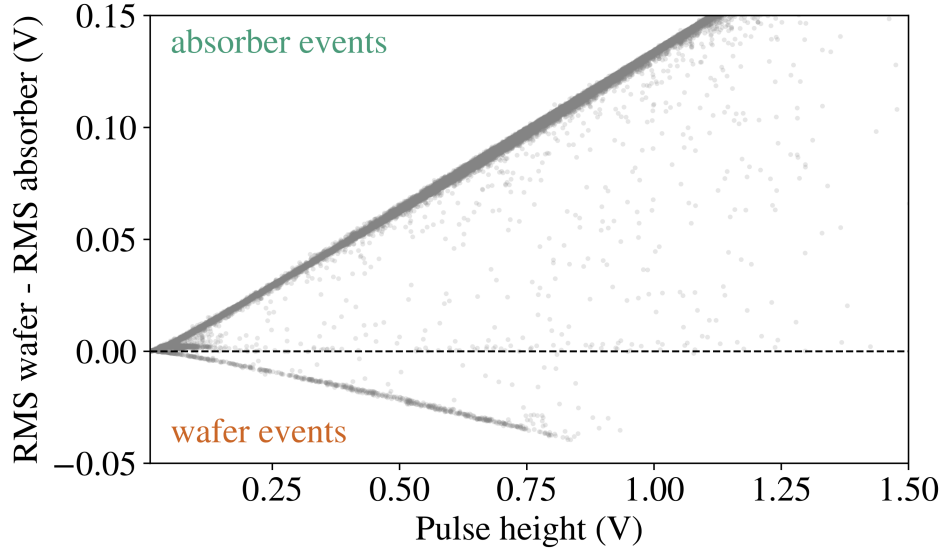


FIG. 4: Difference between RMS values from the wafer SEV fit and the absorber SEV fit as a function of moving-average pulse height for the TeO_2 prototype; different event bands corresponding to the different classes are visible. The event population between the absorber and the wafer band corresponds to the Au hits; its pulse shape is a mixture of the former two classes, and their shapes match it equally well.

Absorber material	"Absorber" events	"Wafer" events	"Gold" events
Si	6072	398	-
TeO_2	28555	711	314

TABLE II: Number of surviving events after quality cuts for each measurement and event class (see text for details).

B. Energy calibration and resolution

The K_α peak from the ^{55}Fe source (5.89 keV) prominent in the spectrum of the Si and TeO_2 detector is used to calibrate the detector response, which is given by the truncated fit result for absorber events corrected by the heater response information. We chose the truncated fit over the usual method of optimal filtering [24] here, since the noise conditions in both measurements changed over time, and the filter relies on a stable noise power spectrum. The resulting spectra for absorber events are given in Figure 5.

The baseline resolution is determined for each detector in the following way: in each measurement, records without a trigger event are taken in regular intervals. These "empty baselines" are then cleaned, removing random coincidences with pulses and artifacts. Subsequently, we superimpose the SEV for a given detector with all remaining empty baselines. These artificial events (122 for the Si detector and 1932 for TeO_2) are passed through the analysis chain and reconstruction algorithm, and the detector resolution is extracted from the reconstructed amplitudes assuming that the noise fluctuations follow a Gaussian distribution. The resolutions (all in σ) are (18.4 ± 1.2) mV for the Si and (1.22 ± 0.02) mV for the TeO_2 absorber, corresponding to (87.8 ± 5.6) eV and (193.5 ± 3.1) eV, respectively (cf. Table I). Typically, the achievable threshold of a TES is about five times the baseline resolution.

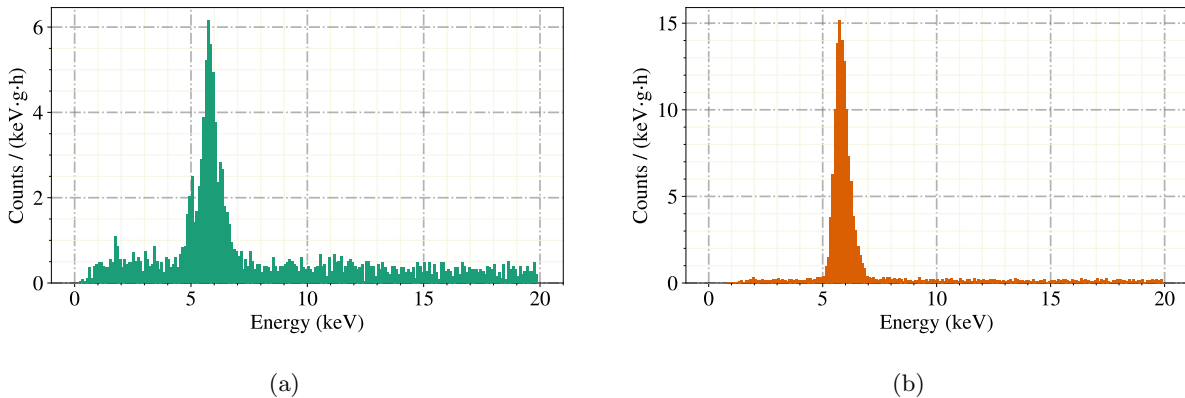


FIG. 5: The energy spectra of the two prototype detectors: (a) Si absorber and (b) TeO_2 absorber. The intensity of the ^{59}Fe -source producing X-rays of 5.89 keV (K_α) and 6.49 keV (K_β) was significantly stronger for (b). The additional peaks in the Si detector (~ 1.8 keV and ~ 5 keV) are consistent with x-ray emission from the K-shell of Si (1.84 keV), and an escape line due to the Cu holder (Cu L_α at 0.93 keV).

IV. CONCLUSION

The *remoTES* is an alternative design of the TES coupling to the absorber in a cryogenic calorimeter. It can be used in combination with delicate absorber materials such as NaI, which cannot withstand the process of direct TES fabrication. In this work we presented the successful operation of two *remoTES* detector prototypes using a Si and a TeO_2 absorber in above-ground measurements, achieving baseline resolutions of 87.8 eV and 193.5 eV, respectively. We observed two event classes with distinctively different pulse shapes in each detector, which result from particle interactions in the absorber and in the wafer of the TES. Additionally, a third event class was visible in the TeO_2 measurement, which featured a very low rate and long decay time, consistent with hits in the gold pad glued onto the TeO_2 absorber. We already performed first measurements with NaI absorbers which are subject of future publications. Compared to “composite-type” detectors, the *remoTES* improves phonon propagation from the absorber to the sensor, if absorber and carrier are made of different materials ([25]). This design additionally prevents the undesirable collection of scintillation light in the carrier. Furthermore, the separately fabricated wafer-TES can be reused with a different target – this implies an improved reproducibility for *remoTES* detectors with respect to their carrier design counterparts, and greatly facilitates comparisons between different absorber materials. In summary, our results show that the TES technology can be successfully used with almost any absorber material, and that *remoTES* detectors are well suited for cryogenic rare event searches. Indeed, absorber materials that required the use of a carrier crystal in the past can now be operated without such a crystal by simply adding a gold interface. Even for “standard” absorbers, the use of a *remoTES* avoids exposing the material to fabrication processes, thus preserving the initial radiopurity and lattice condition of the absorber crystal.

ACKNOWLEDGMENTS

This work was carried out in the frame of the COSINUS collaboration. We would like to acknowledge Matt Pyle, Eneclali Figueroa-Feliciano and Bernard Sadoulet who had the idea of developing such-kind of TES-based detectors, as published already in 2015 on arXiv:1503.01200 [12]. The data analysis was mainly carried out with collaboration-internal software tools, and partially with the open source Python package CAIT[26]. We want to thank the MPP mechanical workshop team for in-time support in all needs regarding the cryogenic facility and detector holder fabrication. We are grateful to the colleagues from the CRESST MPP group for sharing the infrastructure for detector production, the wet dilution refrigerator facility for the measurements and their cryogenic expertise and experience. In particular we thank Ahmed

Abdelhameed for many insightful discussions on thin-film technology.

-
- [1] A. Abdelhameed et al. First results from the CRESST-III low-mass dark matter program. *Phys. Rev. D*, 100(10):102002, Nov. 2019. doi:10.1103/PhysRevD.100.102002.
- [2] I. Alkhatib et al. Light Dark Matter Search with a High-Resolution Athermal Phonon Detector Operated above Ground. *Phys. Rev. Lett.*, 127(6):061801, Aug. 2021. doi:10.1103/PhysRevLett.127.061801.
- [3] R. Agnese et al. Search for low-mass dark matter with CDMSlite using a profile likelihood fit. *Phys. Rev. D*, 99(6):062001, Mar. 2019. doi:10.1103/PhysRevD.99.062001.
- [4] G. Angloher et al. The COSINUS project: perspectives of a NaI scintillating calorimeter for dark matter search. *Eur. Phys. J. C*, 76(8):441, Aug. 2016. ISSN 1434-6044, 1434-6052. doi:10.1140/epjc/s10052-016-4278-3.
- [5] G. Angloher et al. Exploring CE ν NS with NUCLEUS at the Chooz nuclear power plant. *Eur. Phys. J. C*, 79(12):1018, Dec. 2019. ISSN 1434-6052. doi:10.1140/epjc/s10052-019-7454-4.
- [6] J. Billard et al. Coherent neutrino scattering with low temperature bolometers at Chooz reactor complex. *J. Phys. G: Nucl. Part. Phys.*, 44(10):105101, Aug. 2017. ISSN 0954-3899. doi:10.1088/1361-6471/aa83d0.
- [7] G. Angloher et al. Results on MeV-scale dark matter from a gram-scale cryogenic calorimeter operated above ground. *Eur. Phys. J. C*, 77(9):637, Sept. 2017. ISSN 1434-6044, 1434-6052. doi:10.1140/epjc/s10052-017-5223-9.
- [8] P. Adari et al. EXCESS workshop: Descriptions of rising low-energy spectra. *arXiv:2202.05097*, 2 2022. doi:10.48550/arXiv.2202.05097.
- [9] G. Angloher et al. Composite CaWO₄ Detectors for the CRESST-II Experiment. In *AIP Conference Proceedings*, volume 1185, pages 651–654. AIP Publishing, Dec. 2009. doi:10.1063/1.3292426.
- [10] K. E. Gray. Nonequilibrium superconductivity, phonons, and kapitza boundaries. *Springer Science & Business Media*, 65, 2012. doi:10.1007/978-1-4684-3935-9.
- [11] V. Zema. Unveiling the nature of dark matter with direct detection experiments. PhD thesis, Gran Sasso Science Institute, Chalmers U. Tech., 2020. URL <https://inspirehep.net/literature/1813204>.
- [12] M. Pyle et al. Optimized designs for very low temperature massive calorimeters. *arXiv:1503.01200*, 2015. doi:10.48550/arXiv.1503.01200.
- [13] R. Chen. Transition Edge Sensor Chip Design of Modular CE ν NS Detector for the Ricochet Experiment. *arXiv*, 11 2021. doi:10.48550/arXiv.2111.05757.
- [14] V. Alenkov et al. First Results from the AMoRE-Pilot neutrinoless double beta decay experiment. *Eur. Phys. J. C*, 79(9):791, 2019. doi:10.1140/epjc/s10052-019-7279-1.
- [15] Y. H. Kim et al. Measurements and modeling of the thermal properties of a calorimeter having a sapphire absorber. *Nuclear Instruments and Methods in Physics Research Section A: Accelerators, Spectrometers, Detectors and Associated Equipment*, 520(1):208–211, 2004. ISSN 0168-9002. doi:10.1016/j.nima.2003.11.230. Proceedings of the 10th International Workshop on Low Temperature Detectors.
- [16] W. Little. The transport of heat between dissimilar solids at low temperatures. *Canadian Journal of Physics*, 37(3):334–349, 1959. doi:10.1139/p59-037.
- [17] F. Pröbst et al. Model for cryogenic particle detectors with superconducting phase transition thermometers. *Journal of Low Temperature Physics*, 100(1-2):69–104, July 1995. ISSN 0022-2291, 1573-7357. doi:10.1007/BF00753837.
- [18] M. Sisti et al. Massive cryogenic particle detectors with low energy threshold. *Nuclear Instruments and Methods in Physics Research Section A: Accelerators, Spectrometers, Detectors and Associated Equipment*, 466(3):499–508, 2001. doi:10.1016/S0168-9002(01)00801-4.
- [19] J. Karvonen et al. Electron–phonon interaction in thin copper and gold films. *physica status solidi (c)*, 1(11):2799–2802, 2004. doi:10.1002/pssc.200405326.
- [20] S. Hart et al. Phase separation in tungsten transition edge sensors. In *AIP Conference Proceedings*, volume 1185, pages 215–218. American Institute of Physics, 2009. doi:10.1063/1.3292318.
- [21] A. Jain et al. The materials project: A materials genome approach to accelerating materials innovation. *APL Materials*, 1(011002), 2013. doi:10.1063/1.4812323.
- [22] Y. Hinuma et al. Band structure diagram paths based on crystallography. *Computational Materials Science*, 128:140–184, 2017. doi:10.1016/j.commatsci.2016.10.015.
- [23] G. Angloher et al. Limits on WIMP dark matter using sapphire cryogenic detectors. *Astropart. Phys.*, 18(1):43–55, Aug. 2002. ISSN 0927-6505. doi:10.1016/S0927-6505(02)00111-1.
- [24] E. Gatti and P. F. Manfredi. Processing the signals from solid-state detectors in elementary-particle physics. *Riv. Nuovo Cim.*, 9(1):1–146, Jan. 1986. ISSN 1826-9850. doi:10.1007/BF02822156.
- [25] K. Schäffner et al. Particle discrimination in teo2 bolometers using light detectors read out by transition edge sensors. *Astroparticle Physics*, 69:30–36, 2015. doi:10.1016/j.astropartphys.2015.03.008.
- [26] F. Wagner et al. fewagner/cait: v1.0.0, July 2021. URL <https://doi.org/10.5281/zenodo.5091416>.